Supplementary Figures 1-20

Supplementary Figure 1

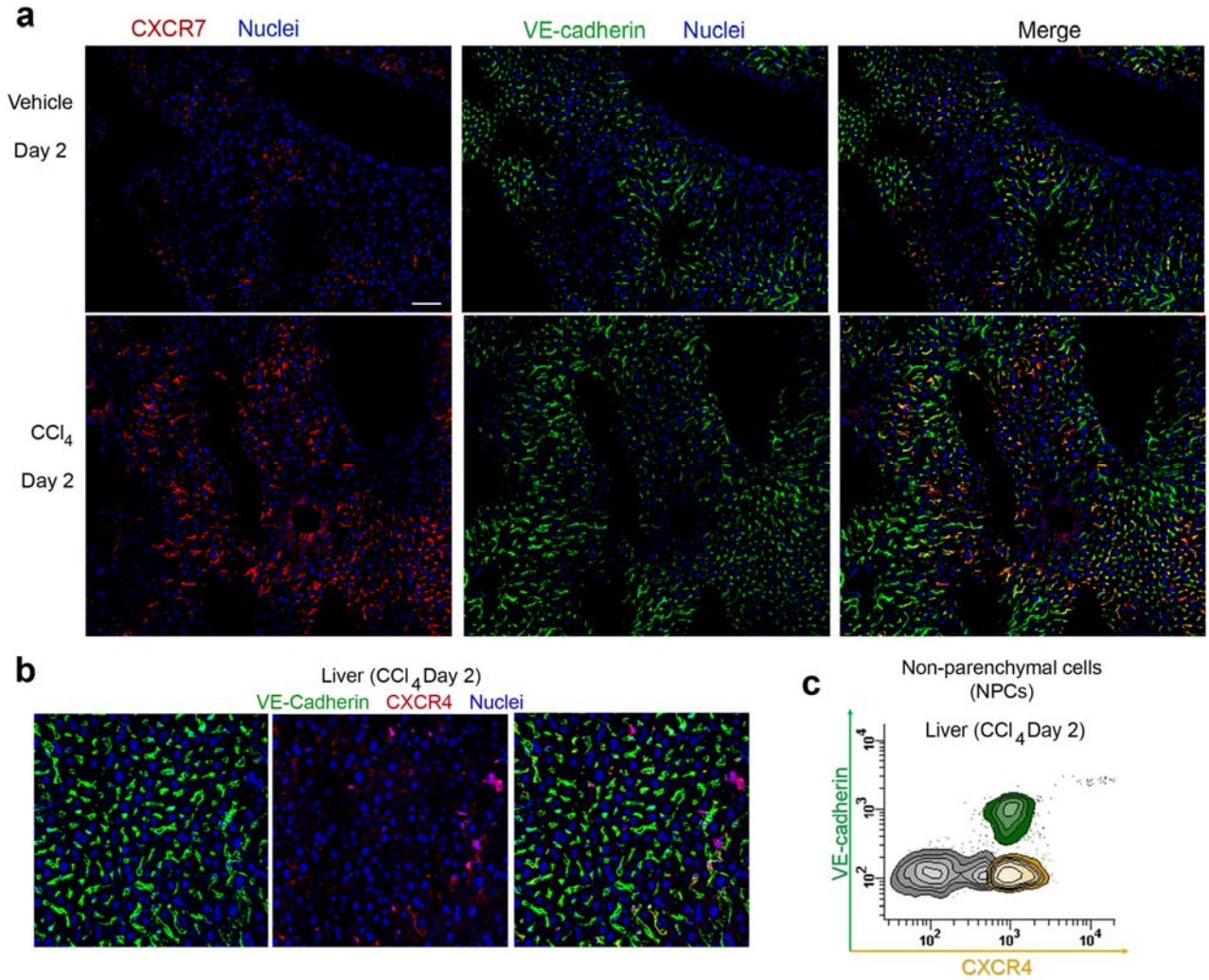

Supplementary Figure 1. Specific upregulation of stromal-derived factor (SDF-1) receptor CXCR7 in mouse liver sinusoidal endothelial cells (LSECs) after acute liver injury.

a) Significantly enhanced expression of CXCR7 on LSECs by single CCl_4 injection, compared to mice administered with vehicle. Two days after intraperitoneal (i.p.) CCl_4 injury, expression of CXCR7 was determined on liver sections. Liver cyrosections were stained for CXCR7 (red fluorescence) and endothelial cell (EC)-specific marker VE-cadherin (green fluorescence). There was a global upregulation of CXCR7 on VE-cadherin$^+$ LSECs by injection of CCl_4 at day 2. Scale bar = 250 μm.

b, c) Expression of SDF-1 receptor CXCR4 in the liver after CCl_4 injury. Two days after i.p. CCl_4 injection, expression of CXCR4 was also examined on liver sections by immunostaining (b) and flow cytometry (c) for CXCR4. Note the expression of CXCR4 on both VE-cadherin$^+$ ECs and VE-cadherin$^-$ non-ECs.

Supplementary Figure 2

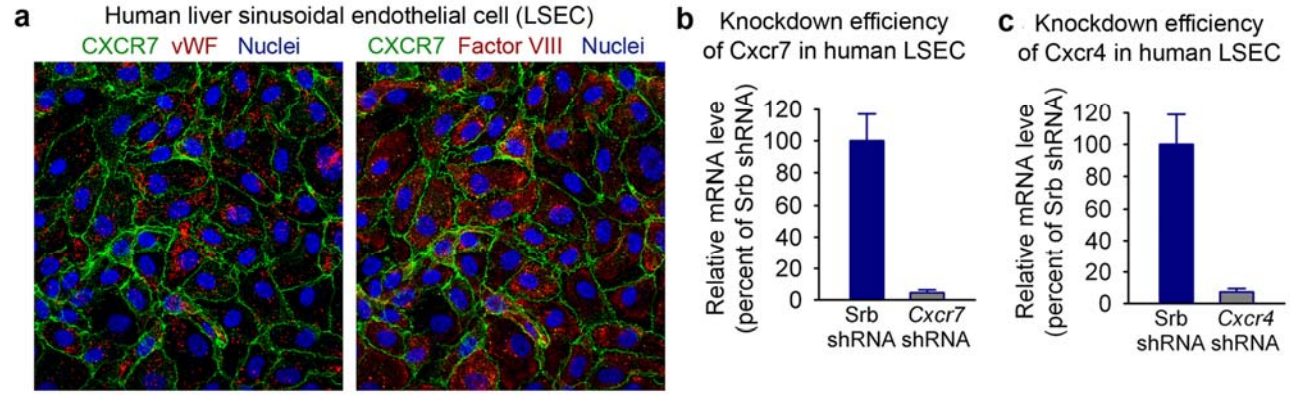

Supplementary Figure 2. Selective knockdown of *Cxcr4* and *Cxcr7* in cultivated human LSECs.

a) Characterization of cultivated human LSECs. Early passages of human LSECs were utilized for deciphering SDF-1 signaling. Human LSECs express surface receptor CXCR7, LSEC-specific marker von Willebrand factor (vWF) and coagulation Factor VIII. LSECs were obtained from ScienCell Research Laboratories and cultured with provided medium. Magnification: 400 x.

b, c) shRNA-mediated silencing of *Cxcr4* and *Cxcr7* in cultivated human LSEC. Human LSECs were treated with lentivirus encoding shRNA against *Cxcr4* or *Cxcr7* (Openbiosystems). After incubation with lentiviral particles, CXCR7 (b) and CXCR4 (c) levels were determined, and the knockdown efficiency was determined by comparing with LSEC treated with Scrambled (Srb) lentivirus; N = 5 in each group.

Supplementary Figure 3

Raw data of Figure 1f

Human liver sinusoidal endothelial cell (LSEC)

SDF-1	–	+			
shRNA	*Scr*	*Scr*	*Cxcr7*	*Cxcr4*	*Cxcr4* *Cxcr7*
Lane	1	2	3	4	5

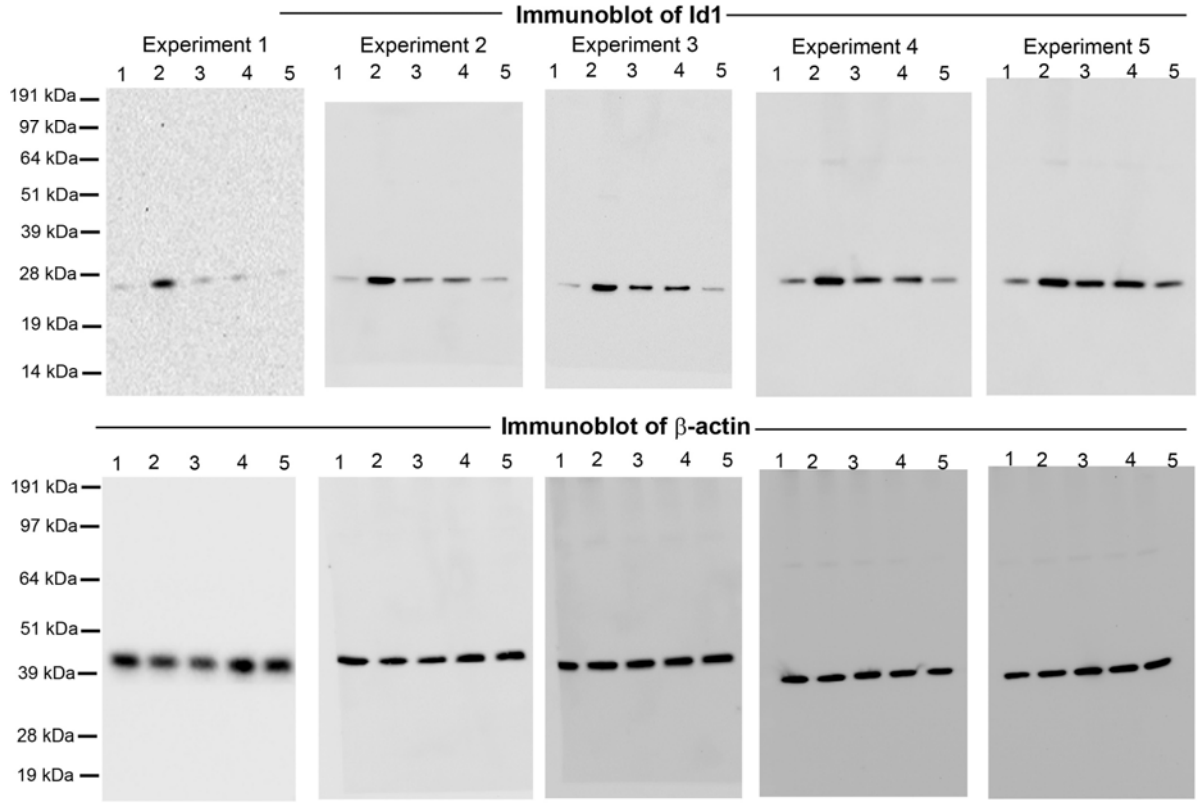

Supplementary Figure 3. Raw immunoblot data presented in Figure 1f that demonstrates the requirement of CXCR4 and CXCR7 in SDF-1-induced upregulation of inhibitor of DNA binding 1 (Id1). Individual immunoblot images with labeled protein markers for five independent experiments presented in Fig. 1f. β–actin was utilized as protein loading control. The expression of Id1 protein was quantified after normalizing to β–actin and presented in Figure 1f bottom panel. These reproducible data demonstrate that shRNA knockdown of *Cxcr4* and *Cxcr7* blocks Id1 induction caused by SDF-1 stimulation.

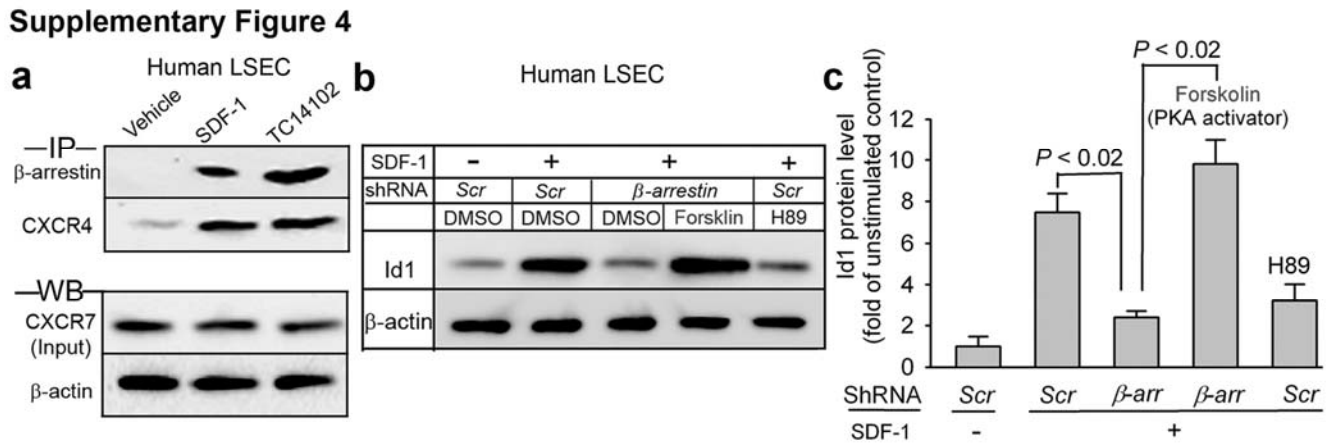

Supplementary Figure 4. SDF-1 and CXCR7-selective agonist TC14102 induce association of CXCR7 with CXCR4 and β-arrestin leading to Id1 upregulation.

a) Immunoprecipitation and Western blot (IP-WB) reveals the association of CXCR4, CXCR7, and β-arrestin in LSECs, upon treatment of SDF-1 and CXCR7-specific agonist TC14102.

b, c) Association of CXCR7, CXCR4, and β–arrestin enables Id1 expression. Genetic silencing of *β–arrestin* inhibited Id1 upregulation by SDF-1, which was restored by protein kinase A (PKA) activator Forskolin. Inhibition of PKA by compound H89 abrogated Id1 upregulation by SDF-1. Representative immunoblot image is shown in (b), and the quantification of Id1 protein level is shown in panel (c). β–arr, β–arrestin shRNA; N= 4.

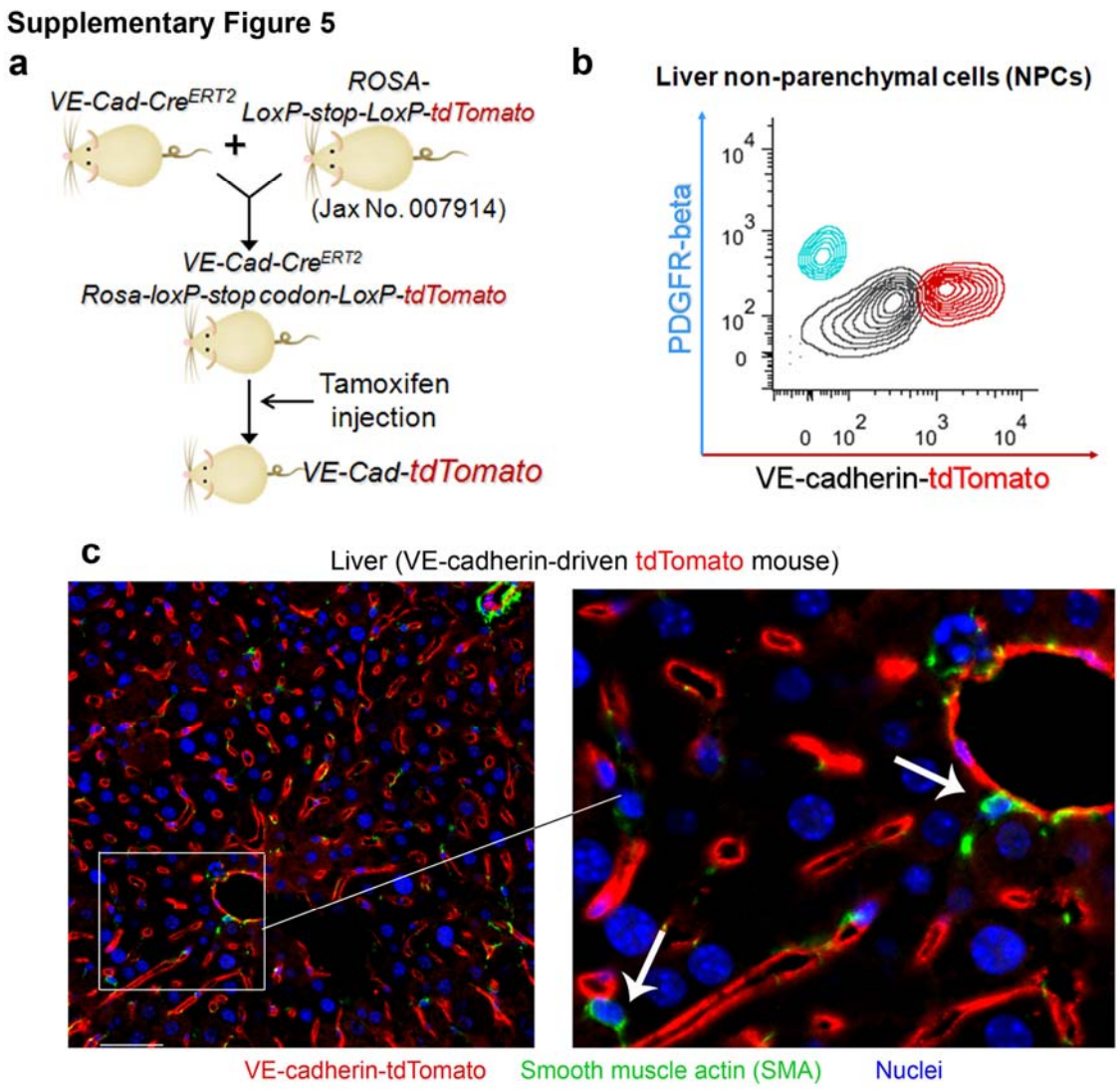

Supplementary Figure 5. VE-cadherin-Cre^{ERT2} is selectively induced in liver endothelial cells (ECs) but not liver cells that are PDGF receptor β^{+} (PDGFRβ^{+}) or α-smooth muscle actin (SMA)$^{+}$.

a) Reporter mouse line that traces the expression of tamoxifen-response Cre^{ERT2} driven by VE-cadherin promoter (*VE-cad-Cre^{ERT2}*). Mice expressing *VE-cad-Cre^{ERT2}* were crossed with reporter mice carrying tdTomato red fluorescent protein following *loxP*-flanked STOP codon. Injection of tamoxifen induced specific excision of "STOP" in VE-cad-Cre^{+}tdTomato^{+} offsprings and expression of tdTomato fluorescent protein in VE-cadherin^{+} cells.

b) *VE-cad-Cre^{ERT2}* does not target hepatic cells that express PDGFRβ**.** Flow cytometry analysis of liver non-parenchymal cells (NPCs). Note that there is no overlap between VE-cadherin-driven tdTomato signals and cells that are positive for PDGFRβ.

c) Co-staining of SMA with *VE-cadherin* driven tdTomato (red fluorescence). Note the distinct localization between tdTomato signal and SMA in the liver. These data indicate that *VE-cad-Cre^{ERT2}* does not target PDGFRβ^{+}SMA^{+} hepatic cells. Scale bar = 50 μm.

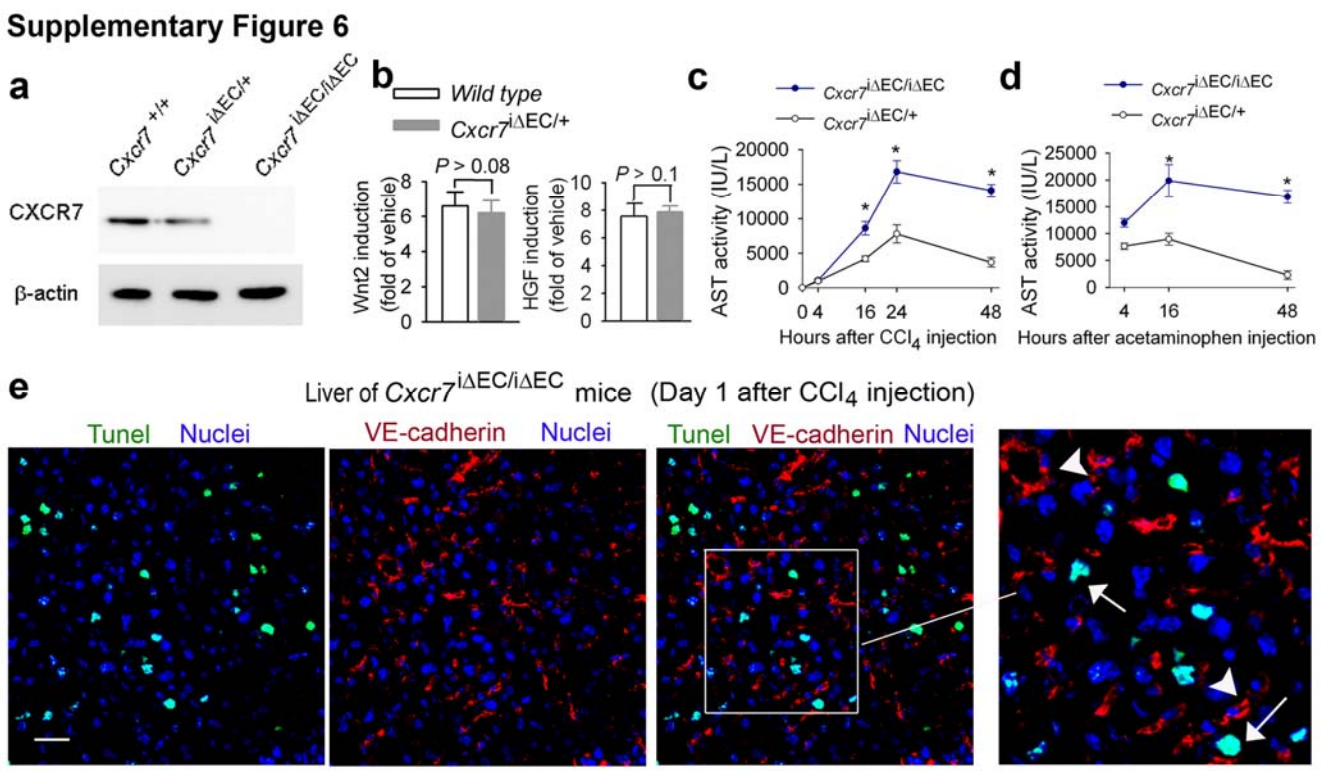

Supplementary Figure 6. Characterization of mice with EC-specific inducible deletion of *Cxcr7* (*Cxcr7*$^{iΔEC/iΔEC}$) using *VE-cad-Cre*^{ERT2}.

a) Inducible EC-specific genetic deletion of *Cxcr7* (*Cxcr7*$^{iΔEC/iΔEC}$) in adult mice using *VE-cad-Cre*^{ERT2}. Mice harboring loxP-flanked *Cxcr7* were crossed with *VE-cad-CreER*^{T2}. EC-specific ablation of *Cxcr7* was induced by tamoxifen injection into the resultant Cre^{+}*Cxcr7*$^{loxP/loxP}$ or Cre^{+}*Fgfr1*$^{loxP/loxP}$ mice. Protein level of CXCR7 was analyzed in LSECs isolated from mice 14 days after tamoxifen injection. This *VE-cad-Cre*^{ERT2} deletion system led to specific ablation of *Cxcr7* in adult mouse LSECs.

b) Regenerative response after acute liver injury is not affected in *Cxcr7*$^{iΔEC/+}$ control mice, compared to wild type (*Cxcr7*$^{+/+}$) mice**.** Protein levels of hepatic-active factors in LSECs of *Cxcr7*$^{iΔEC/+}$ and wild type mice were compared at day 2 after injury. There was little difference in the deployment of hepatocyte growth factor (HGF) and Wnt2 from LSECs. Thus, *Cxcr7*$^{iΔEC/+}$ mice that possess *Cxcr7* EC haplodeficiency represents ideal mouse genotype to control for Cre toxicity; N = 4.

c, d) Liver injury caused by single injection of CCl_4 (c) and acetaminophen (d) is exacerbated in *Cxcr7*$^{iΔEC/iΔEC}$ mice. There was significant increase in the serum level of aspartate aminotransferase (AST) activity at indicated time points; *, $P < 0.05$, compared to control group; N = 4.

e) Absence of EC cell death in *Cxcr7*$^{iΔEC/iΔEC}$ mice after liver injury**.** TUNEL assay was performed in the liver of *Cxcr7*$^{iΔEC/iΔEC}$ mice at day 1 after CCl_4. The majority of apoptotic cells (green fluorescence) were non-VE-cadherin cells, such as hepatocytes (white arrow). Apoptosis was undetectable in VE-cadherin^{+} LSECs (red fluorescence, arrow head). TUNEL assay was performed using In Situ Cell Death Detection Kit (Roche); Scale bar = 50 μm.

Supplementary Figure 7

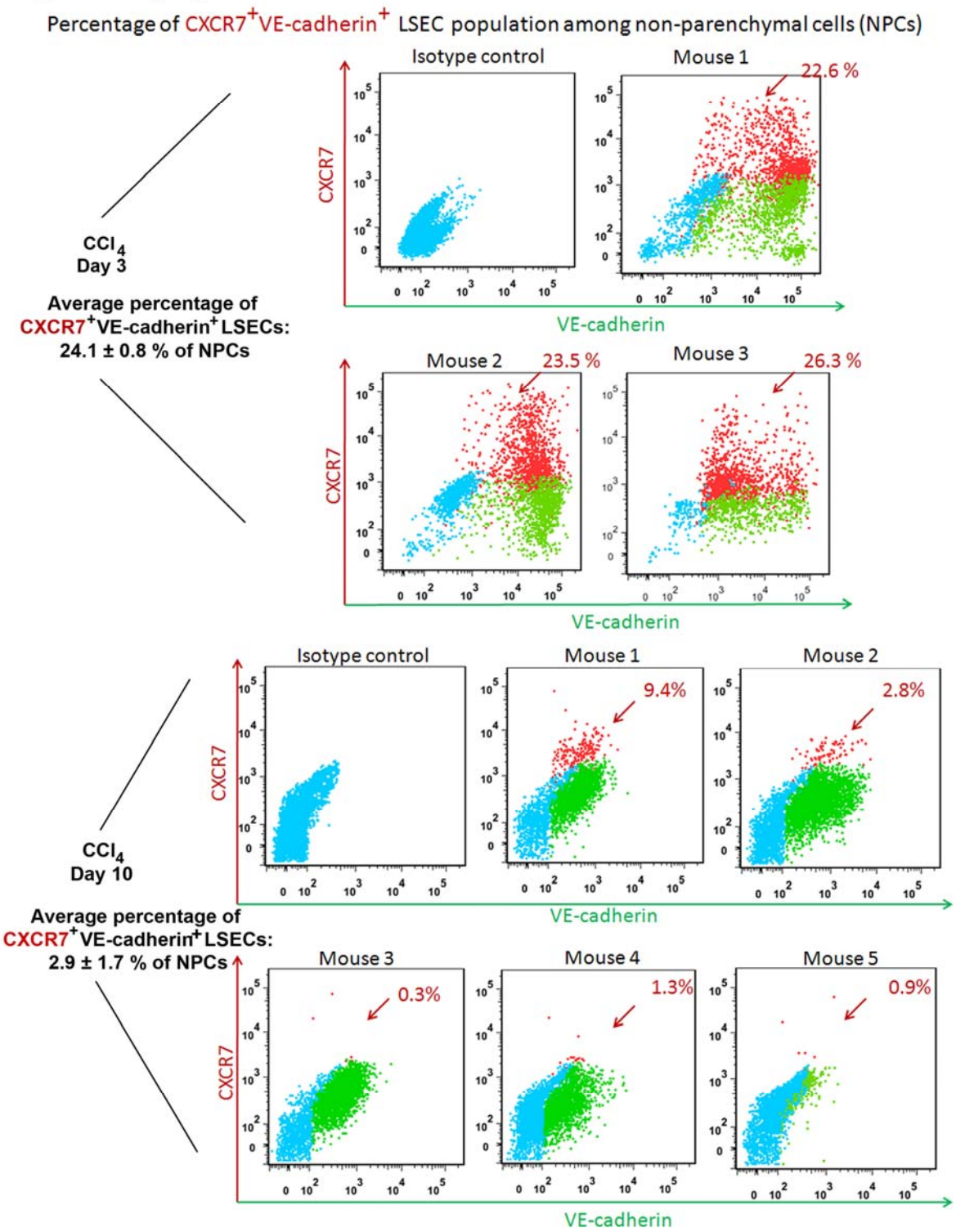

Supplementary Figure 7. Flow cytometry graph presented in Figure 2e. CXCR7 protein level was suppressed in LSECs by repeated CCl_4 injection. Independently repeated experiments presented in Fig. 2e are shown. The percentage of VE-cadherin$^+$ LSECs that express CXCR7 was significantly decreased at day 10 after repeated CCl_4 every three days, relative to that of mouse liver at day 3 after first injection.

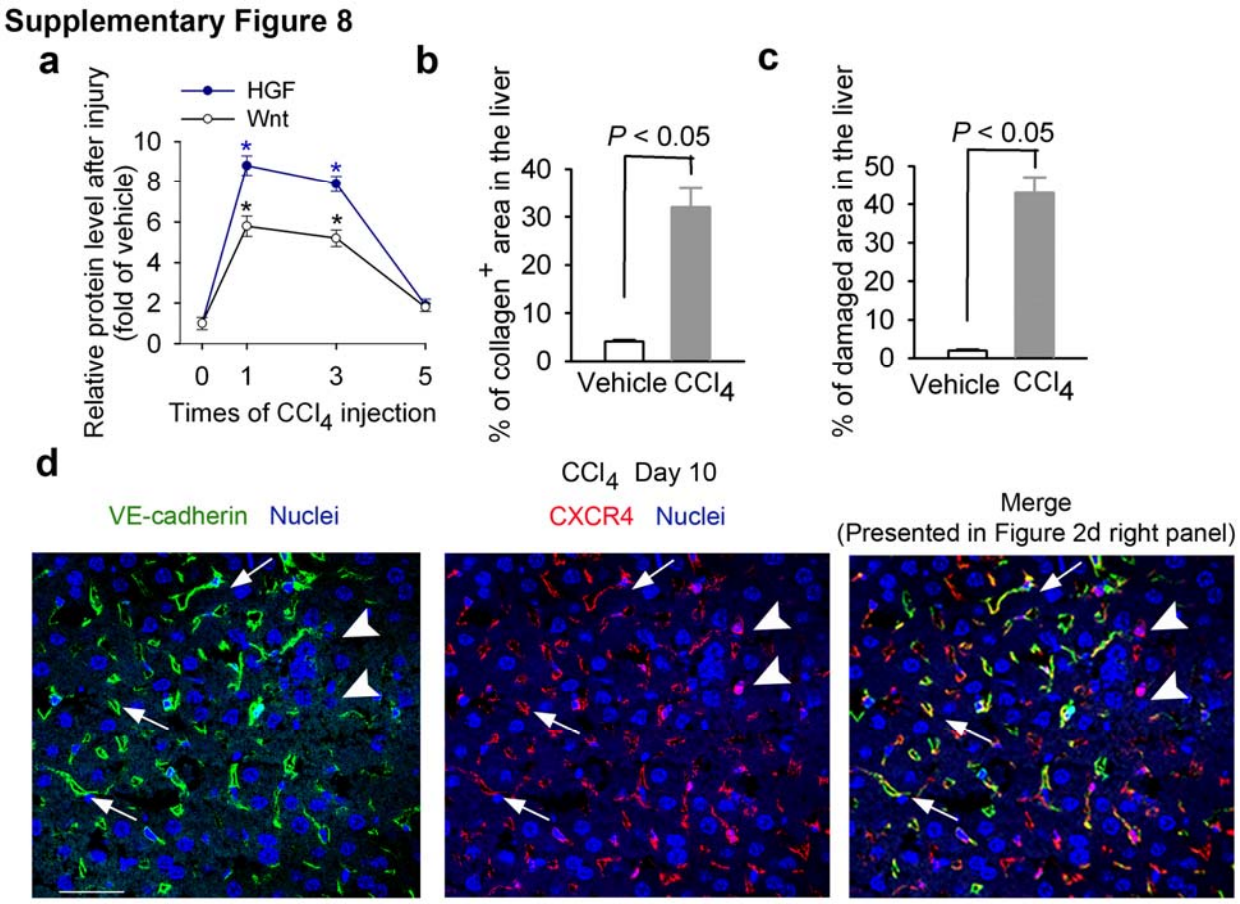

Supplementary Figure 8. Repeated injection of CCl_4 impairs production of pro-regenerative angiocrine factor HGF and Wnt2, leading to fibrotic liver injury.

a) Suppressed production of hepatic-active angiocrine factors HGF and Wnt2 from LSECs by repeated CCl_4 injury**.** CCl_4 was injected to wild type mice every 3 days (Figure 2a). LSECs were isolated from mice at day 2 after the indicated injection time. Quantification of HGF and Wnt2 protein expression demonstrates of the diminished expression of pro-regenerative angiocrine factors by LSECs after 3rd injection of CCl_4; *, $P < 0.05$ compared to vehicle-treated group; N = 4.

b, c) Grade of fibrotic injury caused by repeated CCl_4 injection. Liver damage caused by CCl_4 injury was assessed. Both collagen$^+$ region detected by Sirius red staining (b) and necrotic area were quantified, and compared to vehicle-injected mice; Representative Sirius red staining is shown in Figure 2B; N =5.

d) Immunostaining of CXCR4 (red fluorescence) and liver ECs (VE-cadherin, green fluorescence) on cryosections of CCl_4 injured liver. CXCR4 was upregulated on VE-cadherin$^+$ LSECs (white arrow) and VE-cadherin$^-$ non-ECs (arrowhead) by repeated injection of CCl_4.

Supplementary Figure 9

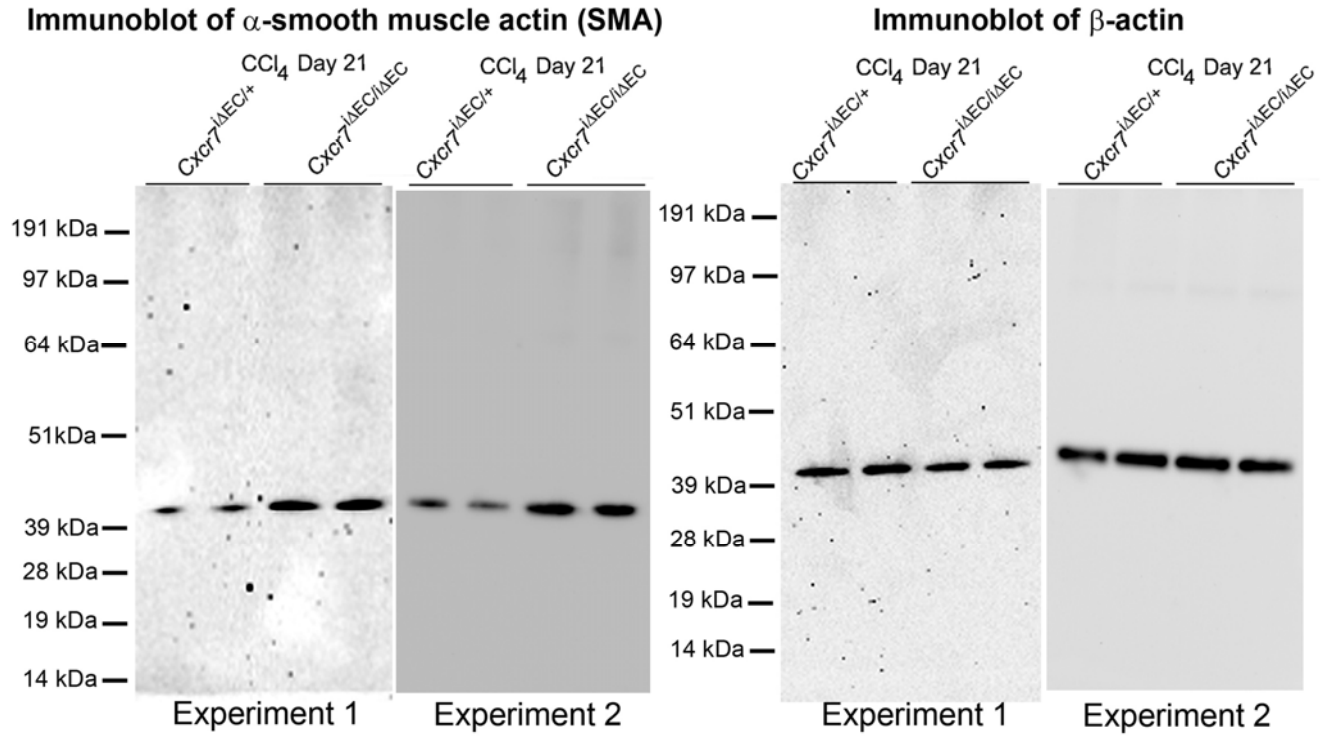

Supplementary Figure 9. Deletion of *Cxcr7* in ECs (*Cxcr7*$^{iΔEC/iΔEC}$) of mice exacerbates liver fibrosis after repeated CCl_4 injection. The degree of liver fibrosis was assessed by immunoblot against SMA expressed by activated myofibroblasts. Raw data of three independent immunoblot images with labeled protein markers are presented. β–actin immunoblot served as protein loading control.

Supplementary Figure 10

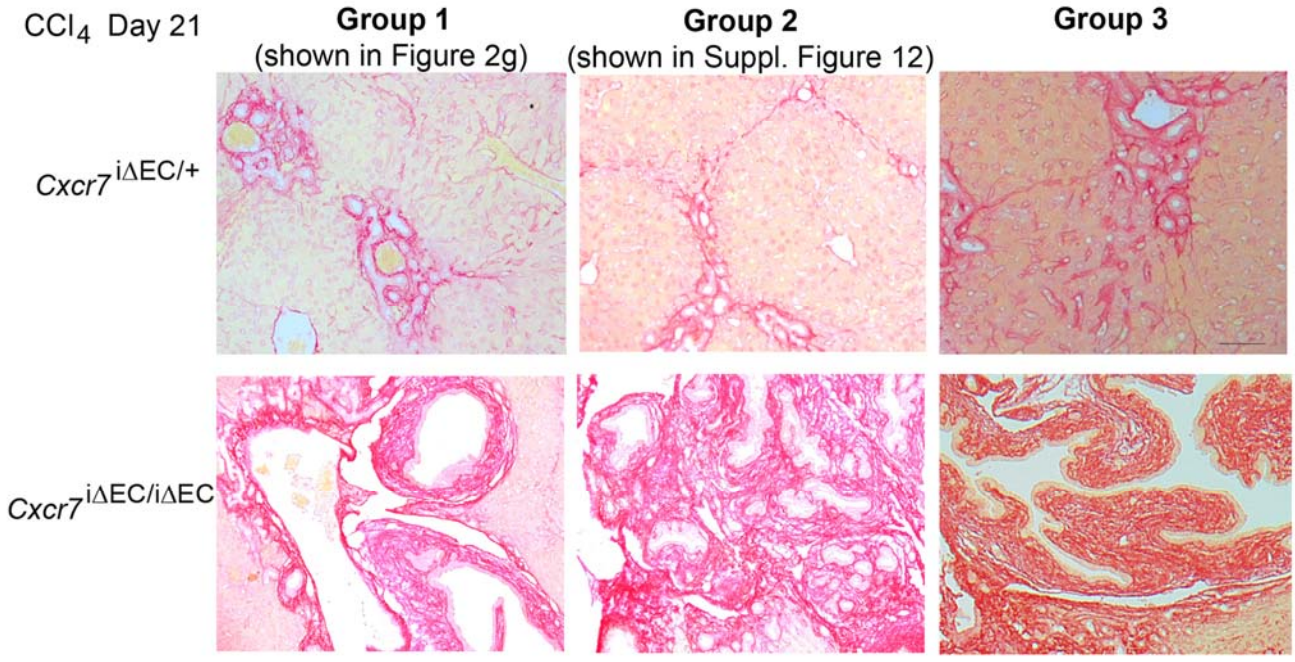

Supplementary Figure 10. Inducible deletion of *Cxcr7* in ECs (*Cxcr7*$^{\mathbf{i\Delta EC/i\Delta EC}}$) increases collagen deposition in the liver after repeated $\mathbf{CCl_4}$ injury. Sirius red staining of *Cxcr7*$^{i\Delta EC/+}$ and *Cxcr7*$^{i\Delta EC/i\Delta EC}$ liver treated with repeated CCl_4. Compared to control *Cxcr7*$^{i\Delta EC/+}$ group, collagen deposition detected by Sirius red staining was markedly enhanced in *Cxcr7*$^{i\Delta EC/i\Delta EC}$ group after repeated CCl_4 injections. Scale bar = 50 μm.

Supplementary Figure 11

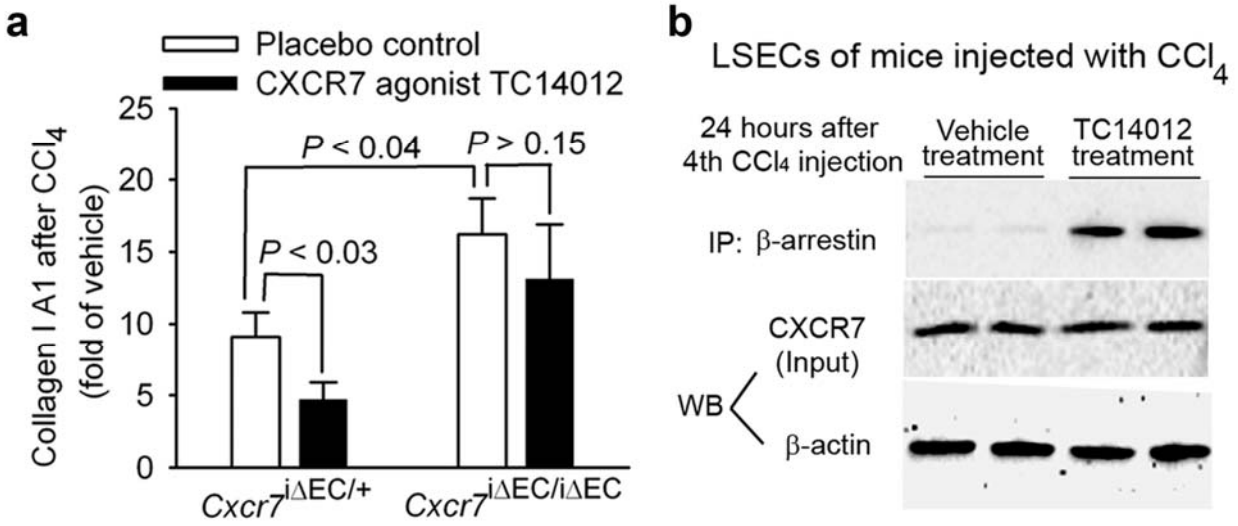

Supplementary Figure 11. Selective activation of CXCR7 by agonist TC14102 in LSECs induces association with β–arrestin after CCl_4 injection.

a) Specific activation of CXCR7 by injection of agonist TC14012 attenuates liver fibrosis. After chronic stimulation of CCl_4, selective CXCR7 activation by TC14012 treatment (30 mg/kg) reduced CCl_4-induced collagen deposition in control but not *Cxcr7*$^{i\Delta EC/i\Delta EC}$ mice. Collagen accumulation was measured by immunoblot (shown in Fig. 2h). Quantification of immunoblot is shown; N = 5.

b) During chronic liver injury, injection of TC14102 leads to interaction of β–arrestin with CXCR7 in LSECs. IP-WB was used to reveal the association of CXCR7 with β–arrestin in LSECs.

Supplementary Figure 12

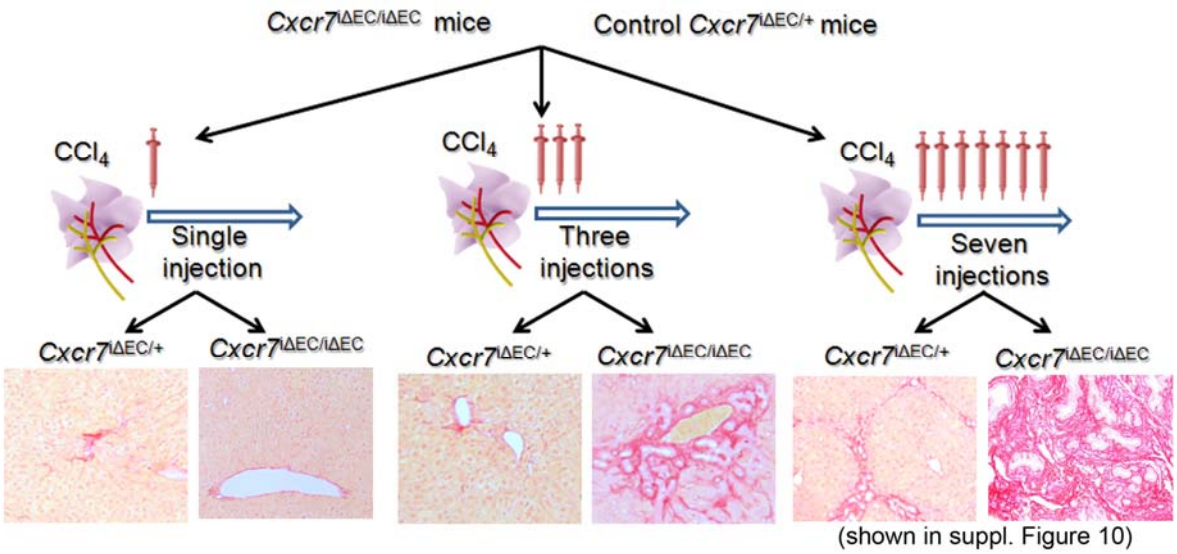

Supplementary Figure 12. Exacerbation of liver fibrosis in *Cxcr7*$^{\text{iΔEC/iΔEC}}$ mice after iterative hepatotoxic injury. Single injection of CCl_4 caused negligible deposition of collagen in both control and *Cxcr7*$^{\text{iΔEC/iΔEC}}$ mice, as evidenced by Sirius red staining. Notably, while three repeated injections of CCl_4 induced little collagen deposition in *Cxcr7*$^{\text{iΔEC/+}}$ mice, *Cxcr7*$^{\text{iΔEC/iΔEC}}$ mice showed significant accumulation of collagen in the liver. The extent of fibrosis was further enhanced in *Cxcr7*$^{\text{iΔEC/iΔEC}}$ mice after seven injections of CCl_4, compared with control *Cxcr7*$^{\text{iΔEC/+}}$ mice.

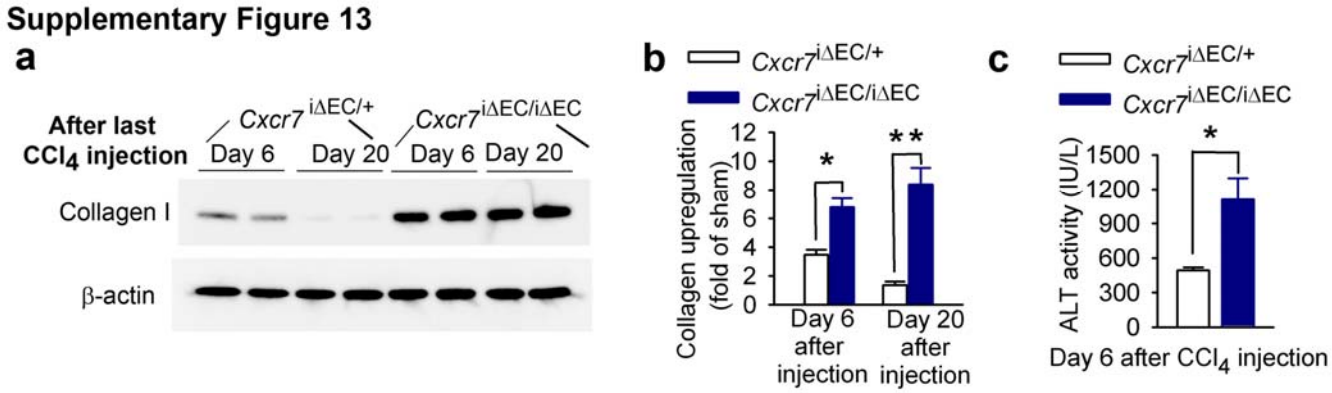

Supplementary Figure 13. Impaired resolution of liver fibrosis in mice that are deficient of *Cxcr7* in ECs (*Cxcr7*$^{iΔEC/iΔEC}$).

a, b) Time-dependent reduction of collagen deposition after liver injury is inhibited in mice with inducible EC-specific deletion of *Cxcr7* (*Cxcr7*$^{iΔEC/iΔEC}$). Schedule of CCl_4 injection was described in Figure 2i. Compared to control mice, there was significantly higher collagen I protein level in *Cxcr7*$^{iΔEC/iΔEC}$ mice. In contrast to the reduced collagen level in control mice at day 20, collagen content after liver injury persisted in *Cxcr7*$^{iΔEC/iΔEC}$ mice.

c) Exacerbated liver injury in mice after liver injury. Serum alanine aminotransferase (ALT) level was markedly enhanced in *Cxcr7*$^{iΔEC/iΔEC}$ mice than that of control mice, suggesting elevated liver damage. These data demonstrate the defective capacity of resolving liver injury in *Cxcr7*$^{iΔEC/iΔEC}$ mice.

Supplementary Figure 14

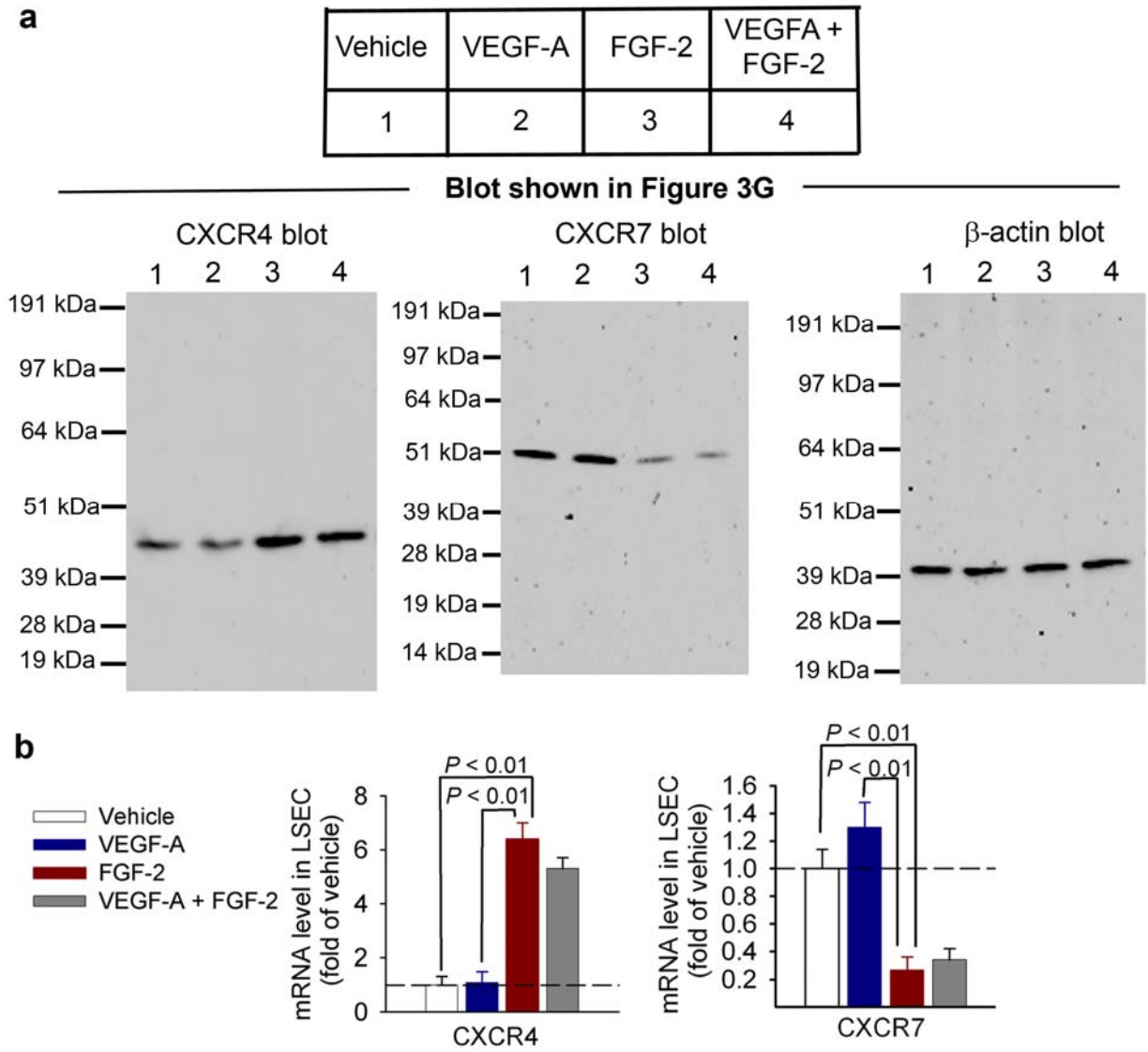

Supplementary Figure 14. FGF-2 treatment leads to CXCR4 upregulation and CXCR7 suppression in LSECs.

a, b) Stimulation of FGF-2, but not VEGF-A, in LSECs caused CXCR4 upregulation and CXCR7 suppression. Representative immunoblot is shown in (a), and quantification of protein level is shown in (b); N=5. LSECs were treated with VEGF-A and FGF-2. Protein levels of SDF-1 receptors CXCR4 and CXCR7 in the treated LSECs were determined by immunoblot.

Supplementary Figure 15

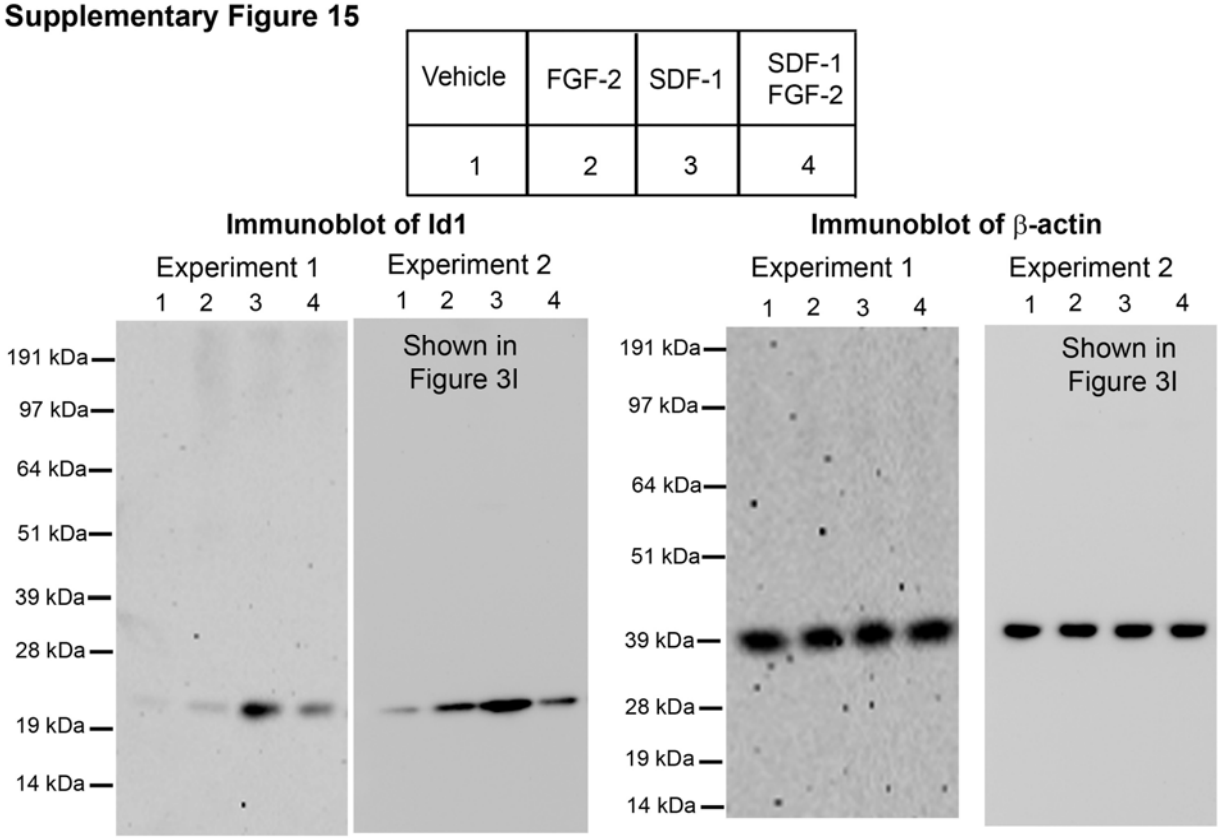

Supplementary Figure 15. FGF-2 antagonizes SDF-1-mediated Id1 in cultivated human LSECs. LSECs were treated with FGF-2, SDF-1, and FGF-2 + SDF-1 combination. Expression of Id1 protein was measured by immunoblot. Two independent immunoblot images are presented. These data demonstrate that FGF-2 inhibits SDF-1-dependent Id1 stimulation.

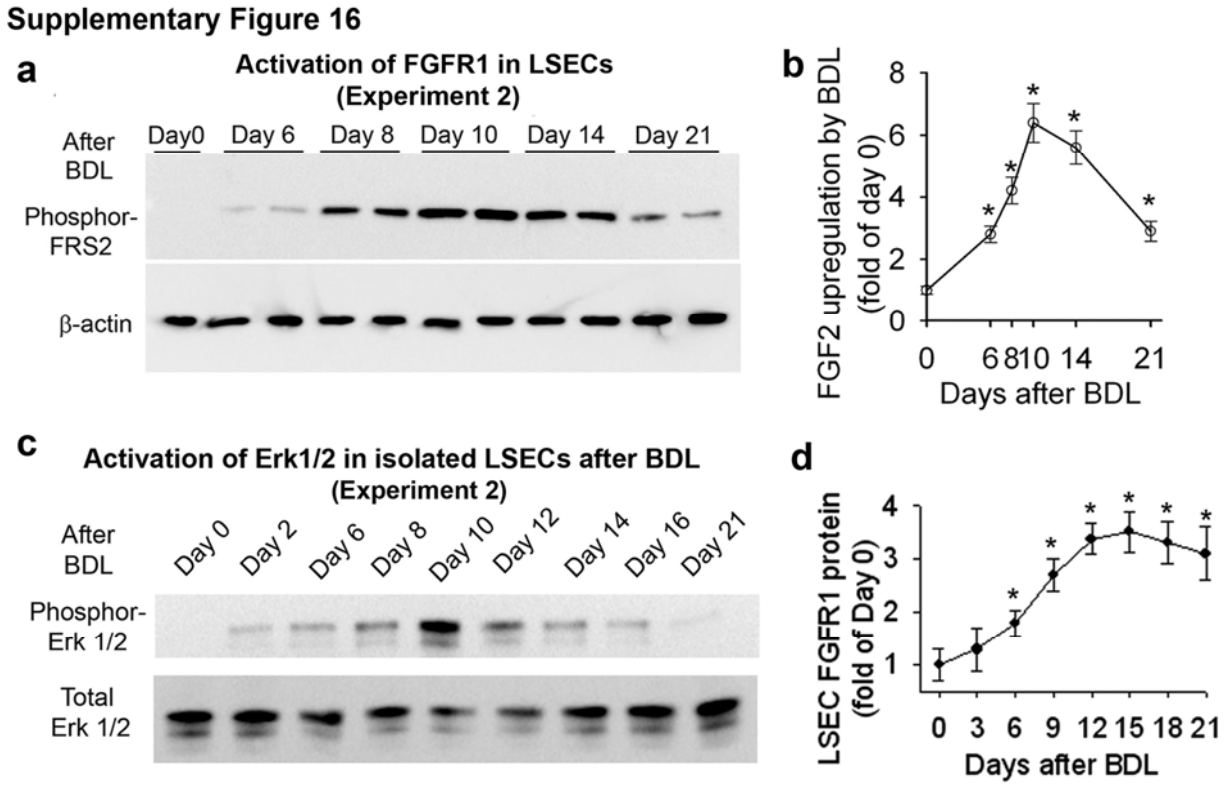

Supplementary Figure 16. During chronic injury FGFR1 overactivation in LSECs leads to pro-fibrotic transition of sinusoidal vascular niche.

a) Time-dependent activation of FGFR1 in LSECs after bile duct ligation (BDL) injury. Phosphorylation of FGFR1 downstream effector FRS-2 (Phosphor-FRS2) was examined in isolated LSECs at different time points to measure the activation of FGFR1. Two independent immunoblot experiments are shown.

b) Increase in FGF-2 protein deposition in the liver after BDL. There is a time-dependent increase of FGF-2 protein level in the injured liver; *, $P < 0.05$, compared with the level at day 0; N = 4.

c) Temporal activation of MAP Kinase (Phosphor-Erk1/2) in LSECs by BDL injury. Erk1/2 phosphorylation in LSECs was examined by immunoblot at different time points after BDL. After normalizing to total Erk1/2, Erk1/2 phosphorylation was assessed.

d) Upregulation of FGFR1 in LSECs after BDL. After BDL LSECs were isolated at indicated time points and the expression of FGFR1 protein was determined. *, $P < 0.05$, compared with the level at day 0; N = 7.

Supplementary Figure 17

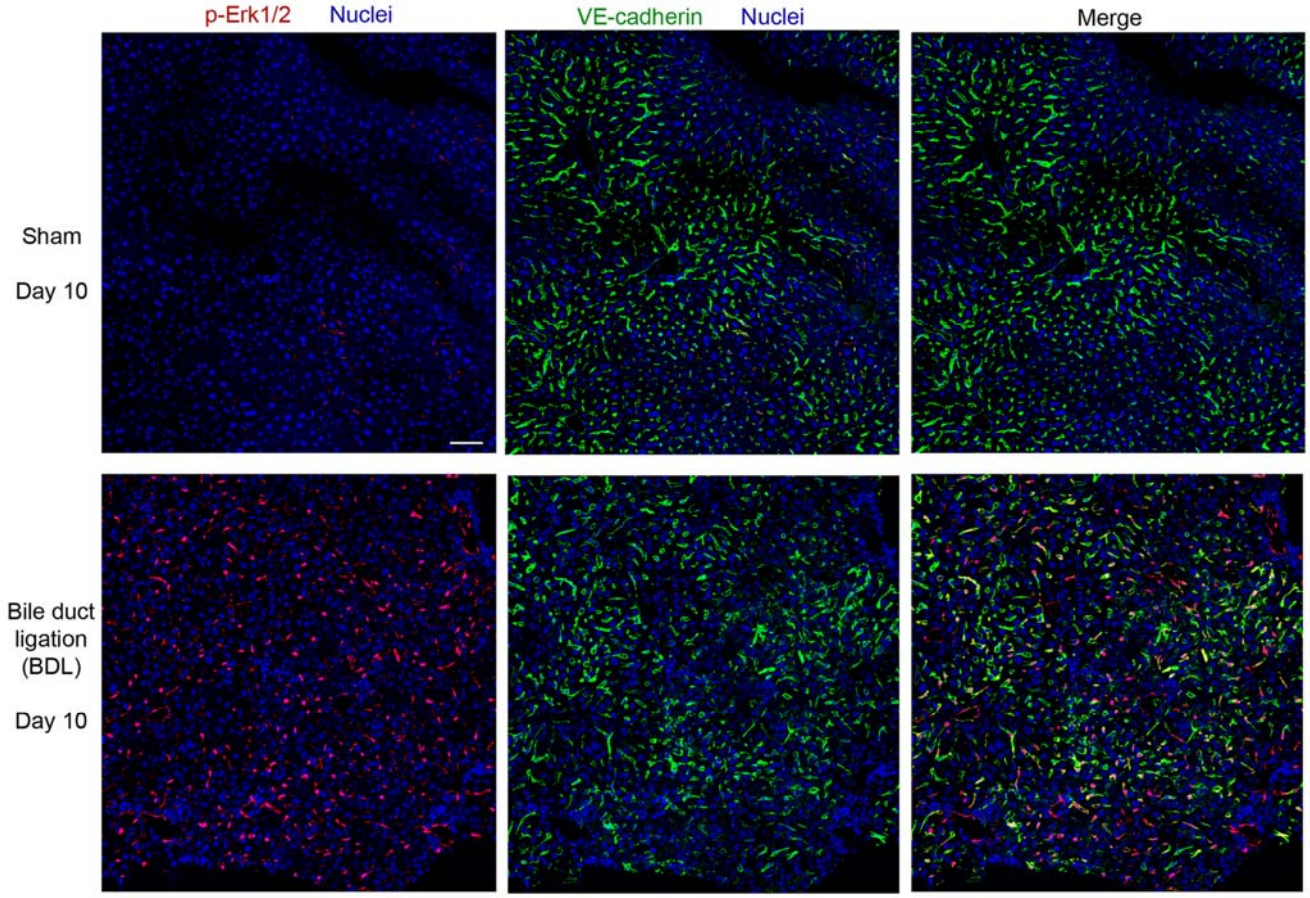

Supplementary Figure 17. Global activation of MAP kinase (Erk1/2) in the liver during chronic injury. MAP Kinase (Erk1/2) is activated/phosphorylated throughout the liver lobe after BDL injury. Phosphorylated Erk1/2 (p-Erk1/2, red fluorescence) was co-stained with VE-cadherin (green fluorescence). Compared with sham-operated mice, bile duct ligation (BDL) caused global appearance of p-Erk1/2 in the liver lobe. Note that the majority of the p-Erk1/2 was localized in the endothelial nucleus. Scale bar = 250 μm.

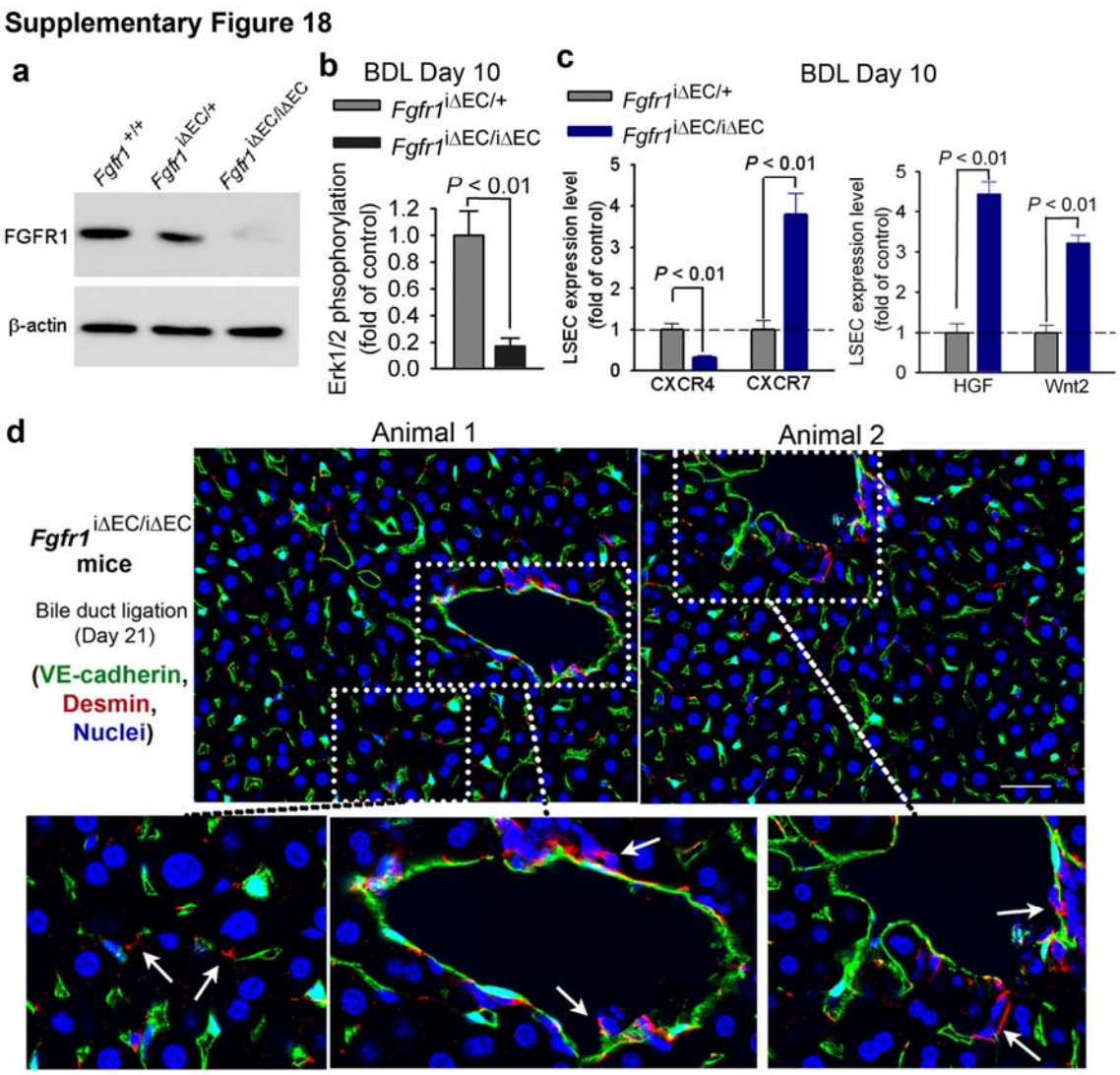

Supplementary Figure 18. Comparable pro-fibrotic responses in wild type (WT) and mice with EC haplodeficiency of *Fgfr1* (*Fgfr1*$^{iΔEC/iΔEC}$).

a) Efficient deletion of *Fgfr1* in LSECs of *Fgfr1*$^{iΔEC/iΔEC}$ mice. Expression of FGFR1 protein in isolated LSECs was determined by immunoblot**.**

b) Inhibition in Erk1/2 activation in LSECs in *Fgfr1*$^{iΔEC/iΔEC}$ mice after BDL. Erk1/2 activation/phosphorylation in LSECs after BDL was determined by immunoblot (Figure 4e). Compared to control mice, Erk1/2 activation was significantly reduced in *Fgfr1*$^{iΔEC/iΔEC}$ mice (F); N =5.

c) Restored pro-regenerative angiocrine response after injury in *Fgfr1*$^{iΔEC/iΔEC}$ mice. Deletion of *Fgfr1* in ECs restored CXCR4 to CXCR7 ratio in LSECs (left panel) and enhanced expression of hepatic-active factors (right panel) in LSECs after BDL; N = 4.

d) EC-specific deletion of *Fgfr1* (*Fgfr1*$^{iΔEC/iΔEC}$) in adult mice attenuates activation and expansion of desmin^{+} fibroblasts after BDL. The distribution of desmin^{+} fibroblasts in the liver of *Fgfr1*$^{iΔEC/iΔEC}$ mice after BDL exhibited a similar pattern to those in the control liver without BDL. By contrast, there was a profound increase in desmin^{+} fibroblasts in the control *Fgfr1*$^{iΔEC/+}$ mice after BDL (as demonstrated by Figure 4b). Scale bar = 50 μm.

Supplementary Figure 19

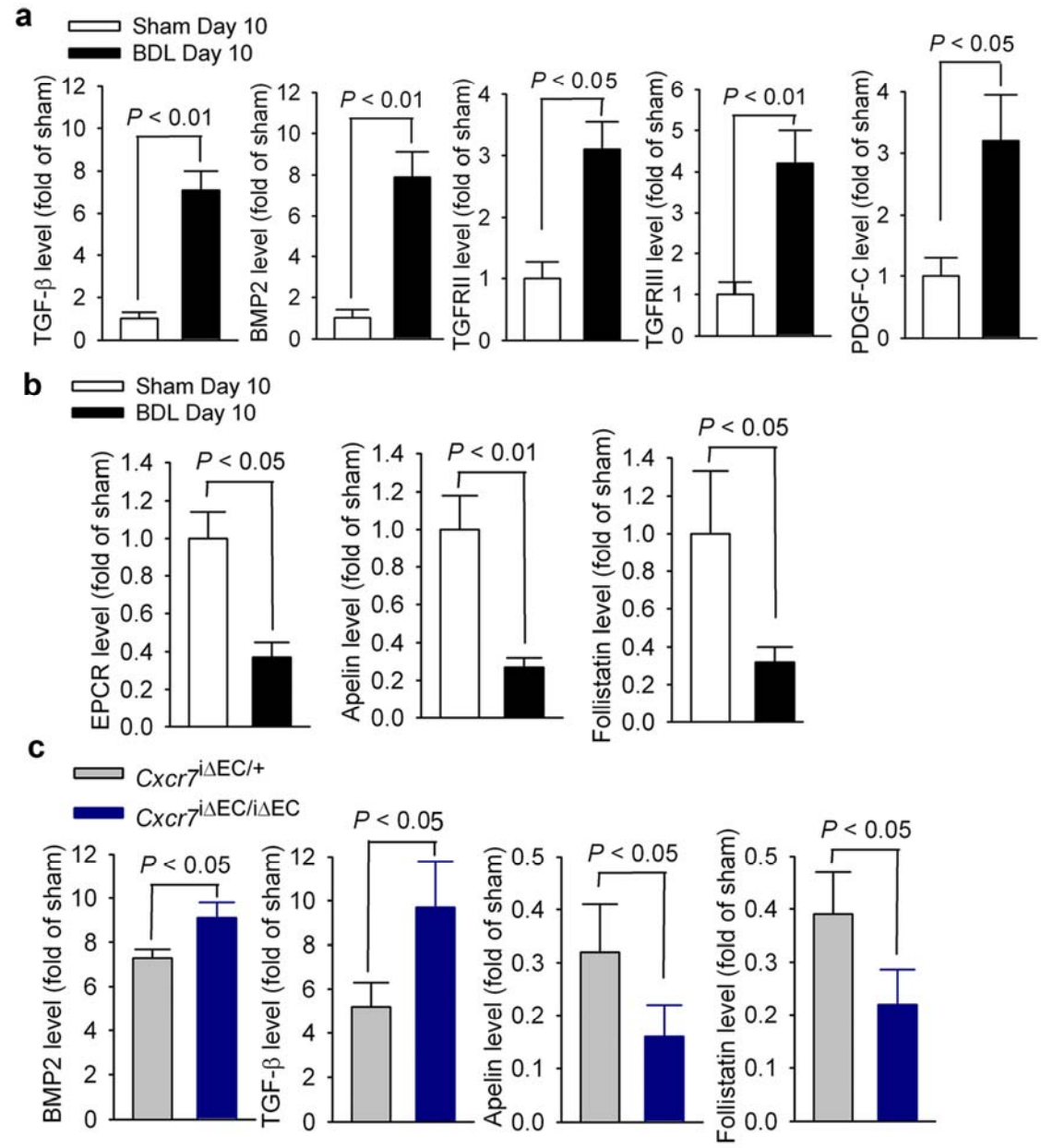

Supplementary Figure 19. CXCR7-mediated pro-regenerative response in LSECs is antagonized by persistent BDL injury, causing pro-fibrotic transition of angiocrine signals.

a, b) Pro-fibrotic shift of angiocrine signals from LSECs after bile duct ligation (BDL) injury. There was a divergent expression of fibrosis-related genes in LSECs after BDL. Factors that regulate BMP and TGF pathways were significantly enhanced (a), and anti-fibrotic genes such as follistatin, apelin, and EPCR were suppressed (b); N = 6.

c) Pro-fibrotic transition of LSECs was exacerbated to a significant extent in *Cxcr7*$^{i\Delta EC/i\Delta EC}$ mice after BDL. Deletion of *Cxcr7* (*Cxcr7*$^{i\Delta EC/i\Delta EC}$) in ECs exacerbated the pro-fibrotic transition of LSECs after BDL; N = 3-5.

Supplementary Figure 20

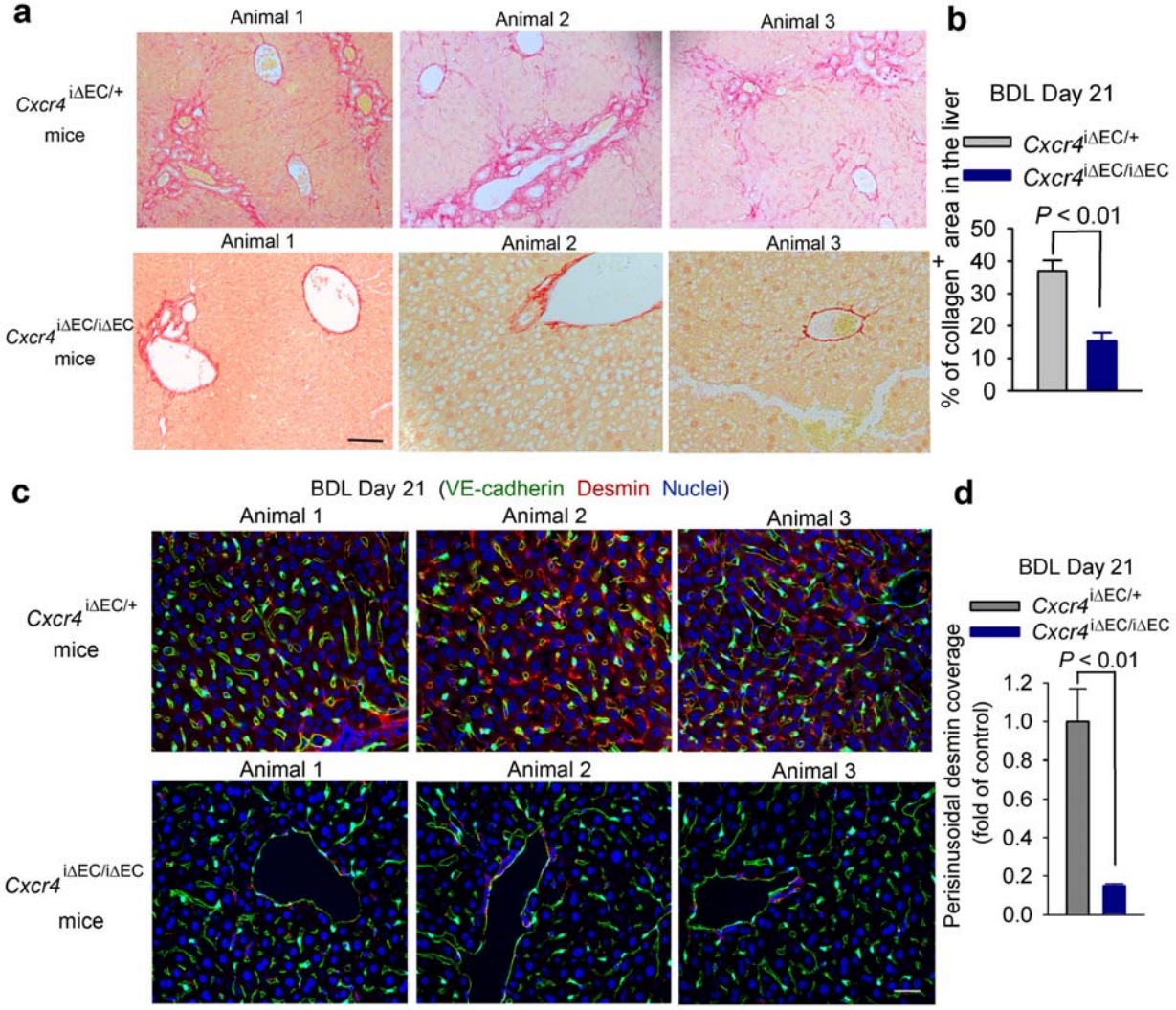

Supplementary Figure 20. Inducible EC-specific deletion of *Cxcr4* in mice (*Cxcr4*$^{iΔEC/iΔEC}$ mice) inhibits liver fibrosis.

a, b) Significantly diminished collagen deposition induced by BDL in the liver of *Cxcr4*$^{iΔEC/iΔEC}$ mice, compared to control *Cxcr4*$^{iΔEC/+}$ mice. Three representative images of Sirius red staining detecting collagen deposition from each group are shown in (a), and quantification of collagen^{+} area is presented in (b). Scale bar = 50 μm. N = 4.

c, d) Perisinusoidal enrichment of desmin^{+} stellate-like is attenuated in *Cxcr4*$^{iΔEC/iΔEC}$ mice. Images of three representative animals from each mouse genotype are presented in C. Quantification of perisinusoidal distribution of desmin^{+} stellate-like cells in the liver is shown (d). Scale bar = 50 μm. N = 4.